small methods
www.small-methods.com

Enhanced Nanoparticle Sensing in a Highly Viscous Nanopore

Taiga Kawaguchi, Makusu Tsutsui, Sanae Murayama, Iat Wai Leong, Kazumichi Yokota, Yuki Komoto, and Masateru Taniguchi*

Slowing down translocation dynamics is a crucial challenge in nanopore sensing of small molecules and particles. Here, it is reported on nanoparticle motion-mediated local viscosity enhancement of water-organic mixtures in a nanofluidic channel that enables slow translocation speed, enhanced capture efficiency, and improved signal-to-noise ratio by transmembrane voltage control. It is found that higher detection rates of nanoparticles under larger electrophoretic voltage in the highly viscous solvents. Meanwhile, the strongly pulled particles distort the liquid in the pore at high shear rates over 10^3 s^{-1} which leads to a counterintuitive phenomenon of slower translocation speed under higher voltage via the induced dilatant viscosity behavior. This mechanism is demonstrated as feasible with a variety of organic molecules, including glycerol, xanthan gum, and polyethylene glycol. The present findings can be useful in resistive pulse analyses of nanoscale objects such as viruses and proteins by allowing a simple and effective way for translocation slowdown, improved detection throughput, and enhanced signal-to-noise ratio.

1. Introduction

Solid-state nanopore is a sensor capable of detecting single molecules and particles in a liquid.[1–4] It monitors the ion transport in a small hole via the ionic current measurements under the applied voltage, which demonstrates pulse-like changes casting the ion blockade characteristics of the objects passing through there.[5] Consequently, it offers a method for identifying individual analytes based on subtle differences in their physical properties, such as size, shape, surface charge density, dipole moments, and mass in a non-destructive fashion.[5,6] In principle, this mechanism can be applied to virtually any substance from cells to genomes by leveraging the various nanofabrication techniques for sculpting a pore that fits their sizes.[7–9] The smaller the objects, however, it usually becomes more difficult to implement the electrical detections. This is because the tiny analytes tend to transit the sensing zone in a quite short time posing difficulty in recording the resistive pulse signals with accuracy due to limitations in the bandwidths of the current amplifiers[10] and the responsiveness of the ionic current.[11] In this context, efforts have been devoted to enhancing the temporal resolution of the ionic current measurement setup.[12,13] Nevertheless, it led to the critical enlargements of the capacitance-derived noise that cannot be removed by conventional bandpass filters as they smear out the fine signal features important for discriminating the analytes.[14]

Slowing down the translocation dynamics has thus been a central challenge in accomplishing nanopore sensing of nanoscale objects such as viruses, proteins, and nucleotides.[15] In general, a multitude of forces affect the translocation motions of objects (neglecting the intriguing interactions at the pore wall surface[16,17]). When an object possesses charges, it can be drawn into a nanopore via the electrostatic forces induced by the focused transmembrane voltage there.[18] If there is a dipole moment, it also contributes to the electrophoretic forces through coupling with the electric field at the nanopore.[19] Hydrodynamic drag force is also important, which can even become a determinant factor when the objects have a scarce amount of charges.[20]

Many strategies have been verified to retard the motions in a nanopore by the fluid properties and external probes to control the forces relevant to the translocation motions. Salt concentration causes a change in the zeta potential, and hence the electrophoretic mobilities, of particles and molecules. Decreasing temperature can retard the fast translocation motions of deoxyribonucleic acid (DNA) via the associated increase in the water viscosity.[21] The pressurized flow is utilized particularly for controlling the capture rates and translocation speed of charge-neutral objects.[22] The fluid flow rate can also be implemented

T. Kawaguchi, M. Tsutsui, S. Murayama, I. W. Leong, Y. Komoto, M. Taniguchi
The Institute of Scientific and Industrial Research
Osaka University
Mihogaoka 8-1, Ibaraki, Osaka 567-0047, Japan
E-mail: tsutsui@sanken.osaka-u.ac.jp
K. Yokota
National Institute of Advanced Industrial Science and Technology
Takamatsu, Kagawa 761-0395, Japan

The ORCID identification number(s) for the author(s) of this article can be found under https://doi.org/10.1002/smtd.202301523

DOI: 10.1002/smtd.202301523

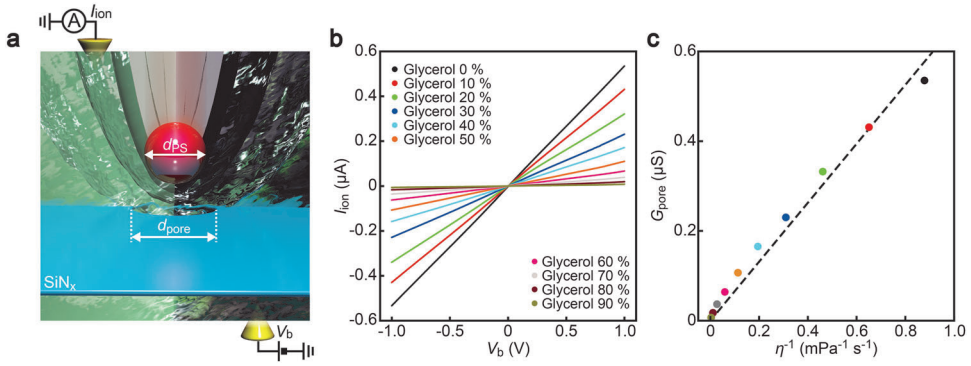

Figure 1. Viscosity dependence of ion transport in a nanopore. a) Schematic illustration depicting polystyrene nanoparticle detection by measuring the ionic current I_{ion} under the transmembrane voltage V_b. d_{PS} and d_{pore} denote the diameters of the polymeric particle and the nanopore, respectively. b) I_{ion} versus V_b characteristics of a 300 nm diameter nanopore in 0.14 M NaCl solution of glycerol-water mixture. The ionic conductance becomes lower when adding more glycerol up to 90 vol%. c) Plots of the nanopore conductance G_{pore} as a function of the inverse viscosity η^{-1} of the electrolyte solutions. A dashed line is a linear fitting with zero intercepts.

by the transmembrane voltage through the electroosmosis,[20] where the membrane surface engineering[23] and the solution pH[24] become important in manipulating its velocity to accelerate/decelerate the translocation dynamics. One can also leverage transmembrane salinity difference in lowering the translocation speed in cases when the ion transport was made charge-selective to generate the ion diffusion-derived voltage across a nanopore.[25] Moreover, optical and electric fields were proven effective in tailoring the fast electrophoresis through the modulated surface charge densities at the membrane surface that changed the contributions of the electroosmosis-mediated hydrodynamic dragging and the electrostatic interactions of the analytes with the pore wall.[26,27] In addition, spot heating by laser irradiation was reported to enable thermophoretic control of DNA via the induced local temperature gradients at nanopores.[28]

Compared to these intricate mechanisms, on the other hand, increasing liquid viscosity by adding organic molecules stands out as the simplest and most effective way for the translocation slowdown.[21,29–34] By merely mixing glycerol in electrolyte buffer, the translocation time of DNA was demonstrated to be extended significantly through the stronger viscous drag forces.[21] Recent experiments have also explored the use of hydrogel and polyethylene glycol to decelerate the translocation motions of protein molecules, making them detectable through ionic current measurements.[29–34] Nevertheless, such efforts aimed at reducing analyte mobility generally entail trade-offs, resulting in diminished detection efficiency and weakened ionic current signals (Figure S1, Supporting Information). Furthermore, it remains to be clarified how the fluid properties impact the translocation dynamics of nanoscale objects and whether their rapid movements affect the local viscosity within a nanopore, which may become significant through the interplay between restricted Brownian motions and liquid shear rates in the nano-confined space. In the present work, therefore, we systematically investigated single-nanoparticle translocation dynamics in organic-water mixtures, uncovering the particle motion-derived shear thickening of the nano-confined fluid that enabled not only the translocation slowdown but also the enhanced detection throughput and signal-to-noise ratio.

2. Results and Discussion

The ionic current I_{ion} through a 300 nm diameter nanopore in a 50 nm-thick silicon nitride membrane[35] showed ohmic behaviors against ramps of the transmembrane voltage V_b in a 0.14 M NaCl buffer of pH 7.4 (**Figure 1a**). Increasing its viscosity by adding glycerol up to 90 vol.% while keeping the salt concentration constant, the $I_{ion} - V_b$ slopes decreased steadily (Figure 1b) due to the diminished ion mobility (glycerol is an organic solvent with the viscosity η amounting 1389 mPa s, which is orders of magnitude higher than that of water (1 mPa s)).[21] Accordingly, the nanopore conductance G_{pore} revealed a quasi-linear relation with η^{-1} (Figure 1c), where we used the empirical formula for estimating the viscosity of the water-glycerol mixtures.[36] Here, the conductance is given by the nanopore geometry (a cylindrical shape with the lithographically-defined diameter d_{pore} of 300 nm and length equivalent to the membrane thickness L_{mem} of 40 nm) and the solution resistivity ρ as $G_{pore} = (R_{pore} + R_{acc})^{-1}$, where $R_{pore} = 4\rho L_{mem}/\pi {d_{pore}}^2$ and $R_{acc} = \rho/d_{pore}$ are the resistance inside and outside the channel, respectively[37] (the contributions of surface counterion conduction is ignored as the effect should be negligibly small for the nanopore much larger than the Dukhin length under the relatively high ion concentration condition and the SiN_x membrane surface charge density of -15 mC m^{-2}).[38] Since the hard dielectric component would be barely deformed under the conditions tested, the change in the ionic conductance is naturally ascribed to the reduced solvent resistivity by the addition of glycerol. In fact, ρ is described as a function of the mobilities of cations (μ_c) and anions (μ_a) as $\rho = n_c e\mu_c + n_a e\mu_a$, where $\mu_{c,a} = Q/6\pi\eta r_{c,a}$ as given by the Stokes law (Q and $r_{c,a}$ are the charge and radii of cations and anions, respectively), which anticipates the linear increase in G_{pore} with the reciprocal viscosity as seen in Figure 1c.

Using this setup, we first investigated the translocation dynamics of nanoparticles in the salt solution without glycerol. Adding 180 nm-sized carboxylated polystyrene nanospheres to one side of the membrane, the ionic current traces exhibited pulse-like changes suggestive of temporal ion transport blockade during their electrophoretic translocation through the nanopore (**Figure 2a**; see also Figures S2–S4, Supporting

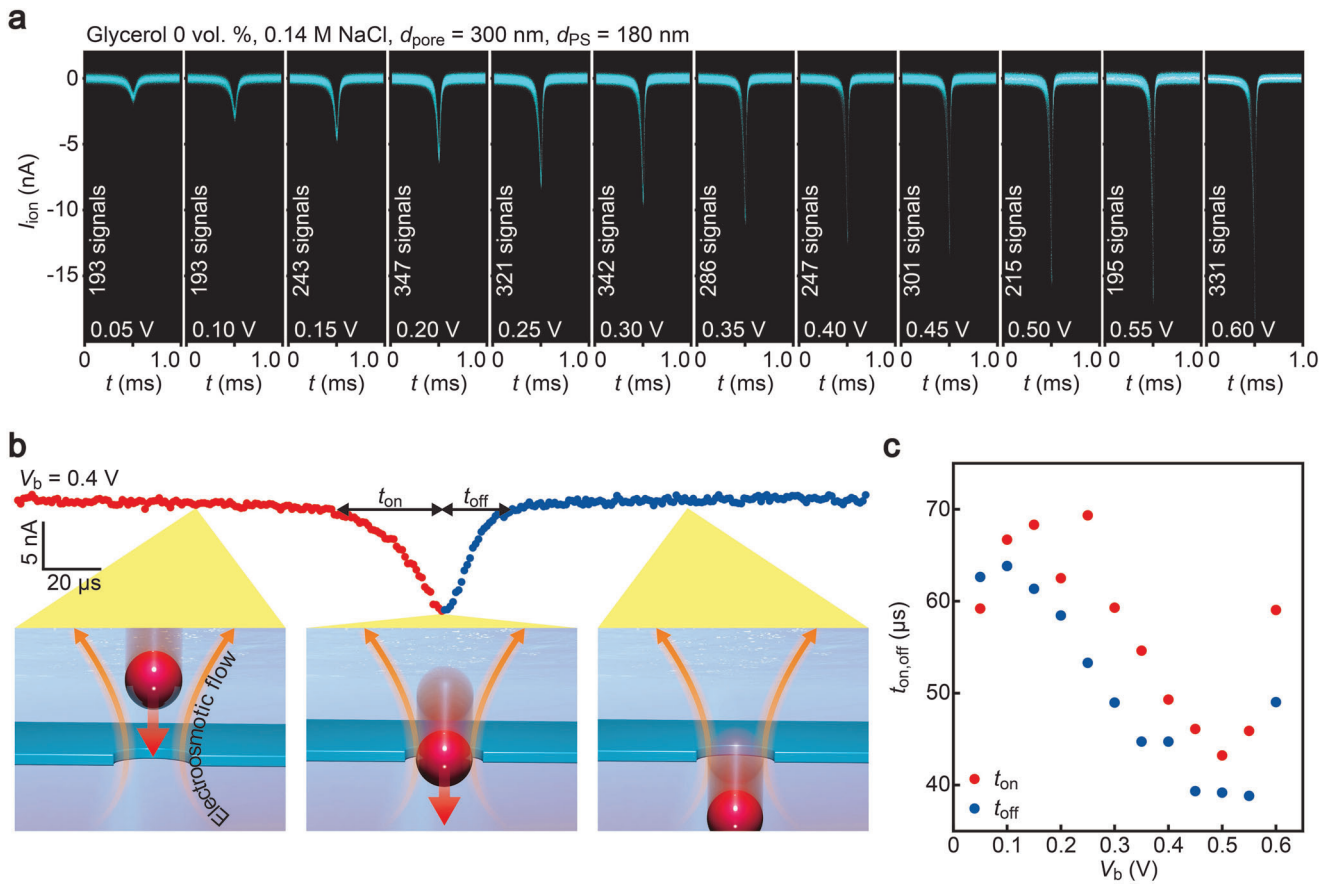

Figure 2. Nanoparticle translocation dynamics in water. a) Resistive pulses recorded in a dispersed solution of 180 nm-sized carboxylated nanobeads in water containing 0.14 M NaCl. The ionic signal becomes larger as the transmembrane voltage is increased from 0.05 (left) to 0.60 V (right). All the data were taken using one identical nanopore. b) A magnified view of a resistive pulse. The insets describe the nanoparticle drawn into the nanopore via the electrophoretic forces (red arrows) against the electroosmotic flow (orange arrows). t_{on} and t_{off} are the capture and escape times, respectively. c) t_{on} (red) and t_{off} (blue) plotted with respect to V_b. While the capture-to-translocation behaviors differ by V_b conditions due to the associated changes in the relative contributions of the electrophoretic and electroosmosis-mediated drag forces, the ratio between t_{on} and t_{off} remains almost unaltered.

Information).[39,40] Upon enlarging the transmembrane voltage from 0.1 V to 0.6 V, the signal intensities increased linearly with V_b in accordance with the transmission line model of the nanopore circuit,[5,41] i.e., the resistance changes in the same manner during the nanoparticle translocation irrespective of the V_b conditions. Closer inspections of the signal profiles identified symmetrical forms of resistive pulses, which is not surprising as the electric field distribution around the nanopore is symmetric with respect to the membrane surface (Figure S5, Supporting Information) that predicts spatiotemporally-symmetric motions of the electrophoretically-driven nanoparticles. To show this quantitatively, we extracted the partial signal widths before (t_{on}) and after (t_{off}) the passage of the nanobeads through the nanopore (Figure 2b; see also Figures S6 and S7, Supporting Information). As shown in Figure 2c, t_{on} and t_{off} tend to become shorter with V_b signifying the faster electrophoretic motions of the nanoparticles under the stronger electric field. An exception is the feature at 0.6 V where the translocation time turns to increase attributed to the more significant increase in the electroosmotic flow speed at that voltage imposing stronger hydrodynamic drag force to slow down the electrophoretic translocation (note that SiN_x surface has negative surface charges at pH 7.4 inducing water flow via the counter-cation transport in direction opposite to the electrophoresis of the negatively-charged polystyrenes).[17] Yet, the ratio between t_{on} and t_{off} remains almost unaltered suggesting the similar contributions of the electrophoretic and electroosmosis-mediated hydrodynamic drag forces on the particle motions at the pore entrance and exit.

In stark contrast to the above observations, we found highly asymmetric resistive pulses in glycerol solutions. Detecting the nanobeads dispersed in glycerol-water mixtures (the salt concentration was kept at 0.05 M), we obtained smaller open pore current I_{open} as well as the ionic signal heights I_p ascribed to the increased liquid viscosity (**Figure 3a**). The stronger viscous drag force on the polystyrenes also led to broadening of the pulse signal waveforms (Figure 3b) and reduced particle capture rates (Figure S8, Supporting Information). Meanwhile, the signal shapes became more asymmetric as we increased the amount of glycerol (Figure 3c). More quantitatively, whereas both t_{on} and t_{off} were found to increase with η indicating the lower mobility of the nanobeads in the more viscous solution (Figure 3d; see also Figures S9 and S10, Supporting Information), the former time

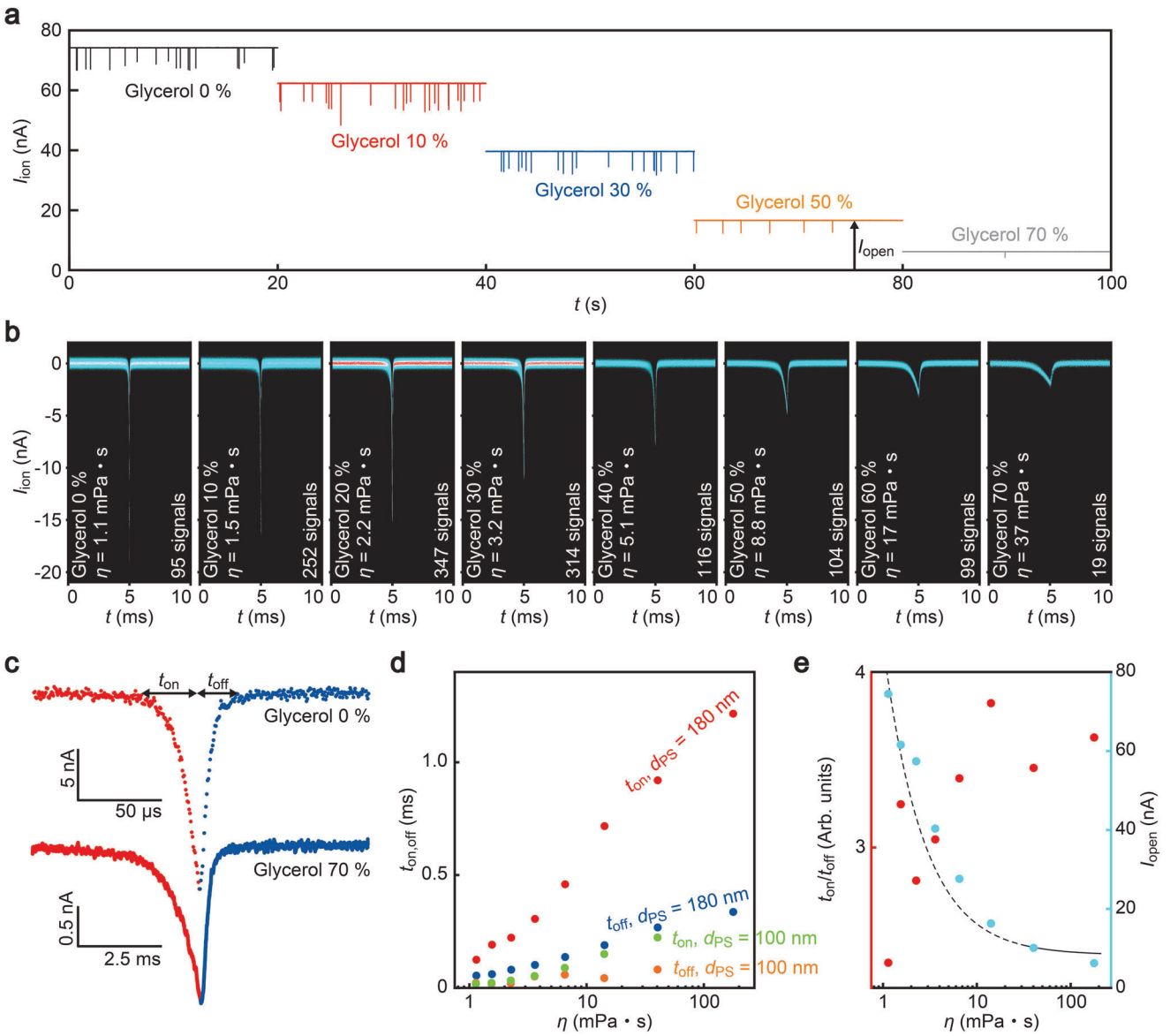

Figure 3. Spatially-asymmetric translocation dynamics in a viscous solution. a) Ionic current traces measured in water-glycerol mixture solutions of 180 nm polystyrene nanoparticles under V_b = 0.2 V. The open pore current I_{open} decreased monotonically with increasing the glycerol contents. b) Resistive pulses observed under different viscosity conditions. All the data were taken using one identical nanopore. c) Magnified views of the ionic signals. As the solution viscosity is increased, the signal waveforms become more asymmetric. Note the difference in the scale of the ionic current and time. d) t_{on} (red) and t_{off} (blue) plotted as a function of η. Results of 100 nm nanoparticles detected with a 150 nm nanopore are also shown. e) The ratio t_{on}/t_{off} plotted as a function of η (red). I_{open} is also shown (skyblue). The dashed curve represents the η^{-1} dependence of the open pore current.

is revealed to be extended more prominently than the latter as shown by the increase in their ratio t_{on}/t_{off} (Figure 3e).

What caused the asymmetric resistive pulses? It is known that capacitance of a nanopore chip couples with the ionic resistance to render a signal retardatio effect like in electric circuits smearing the I_{ion} signals into asymmetric forms by elongating the pulse tails.[11] However, Figure 3b presents signal blunting at its onset and not tail. In fact, we integrated a polyimide micropore layer on the nanopore membrane to reduce the chip capacitance to ensure a fast enough response of I_{ion} to the translocation motions of the polystyrenes.[42] The anomalous asymmetry in the ionic signal profiles should, therefore, originate from the translocation motions of the nanobeads. Meanwhile, since there is no difference in the solution properties at the entrance and exit of the nanopore, the electric potential distribution is theoretically predicted to be symmetric with respect to the membrane plane no matter the viscosity and transmembrane voltage conditions tested (as shown by the finite element analyses in Figure S11, Supporting Information), which expects the narrowing of the ionic signals at both the onsets and tails with V_b as observed in the NaCl solution without glycerol (Figure 2c). Indeed, I_{open} during the resistive pulse measurements (Figure 3e) decreased as η^{-1} ensuring the varied viscosity as settled via the solution preparations. In this regard, inertial effects can be a possible factor that serves to regulate the

passages of the particles toward the axial direction after escaping the nanopore.[43] Nevertheless, their influence is anticipated to be negligible in the liquids much more viscous than water as denoted by the short Stokes time of 51 ps for the 180 nm nanosphere of 3.2 fg in the 70 vol.% glycerol-water solution of η = 37 mPa s. The asymmetric features in the resistive pulses thus suggest peculiar contributions of local viscosity in the nanopore on the electrically-driven translocation dynamics in the organic-water mixtures.

In an effort to shed further light on the mechanism behind the electrokinetic asymmetry, we carried out the resistive pulse measurements in a high-content glycerol solution (80 vol.%) of 0.8 M NaCl under various V_b conditions (**Figure 4**a,b). Here, we utilized the relatively high salt concentration to compensate for the reduction in the ion mobilities associated with the elevated viscosity to gain a large enough ionic current response upon the electrophoretic translocation of the polymeric nanobeads. We found a linear increase in both I_{open} and I_p with the transmembrane voltage (Figure 4c) similar to the results obtained in water (Figure S12, Supporting Information). Furthermore, the nanoparticle capture rates f_{cap}, deduced by a statistical analysis of the occurrence rates of the ionic signals (Figure S13, Supporting Information),[44] became higher under larger V_b ascribed to the more extensive electric field distributions at the pore entrance for electrically drawing them into the nanopore (Figure 4d; see also Figure S14, Supporting Information, for the case in salt water). Curiously, on the other hand, while this anticipates faster electrophoretic speed of the nanoparticles by stronger electric field at the nanopore, the V_b dependence of the resistive pulse width t_d revealed the opposite indicating their slower translocation motions under larger transmembrane voltages (Figure 4b,d; Figures S15 and S16, Supporting Information).

Closer inspections of the signal waveforms (Figure 4e; Figures S17 and S18, Supporting Information) identified slightly shorter t_{off} at higher V_b, denoting faster electrophoretic motions of the polystyrenes under the larger electric field at the pore exit (Figure 4f). On the contrary, t_{on} became longer upon raising the voltage from 0.2 to 1.0 V (Figure 4f; Figures S19 and S20, Supporting Information). Marcuccio et al.[45] observed similar asymmetric resistive pulse signals for DNA electrophoretically translocating through a nanopipette under a viscosity gradient formed with salt solution and a water-organic mixture. They attributed the slow decay of the ionic current to the roles of dense counterions on the polynucleotide chain, along with the complex interactions of the solutions involving shifting of the solution interface.[45] Unlike DNA, in contrast, the contribution of counterions is anticipated as negligible for the 180 nm-sized polystyrene beads having bulky spherical structures that render mostly volume exclusion effects. Moreover, the nanopores in the present work were filled with homogeneous water-organic mixtures of constant viscosities and ion concentrations, and hence there is no solution interface at the nanopore. Therefore, the signal asymmetry observed here cannot be attributed to the physico-chemical interactions of the electrolyte solution. Instead, it is more natural to ascribe the signal asymmetry (Figure 4g) to much slower motions of the nanobeads at the entrance by up to a factor of three than those at the exit. As a whole, it led to the increase in t_d manifesting the significance of the electric-field-mediated translocation slowdown in the capture stage.

To better understand the counterintuitive translocation behaviors, we deduced their real-time dynamic motions from the resistive pulse profiles. For this, we simulated the I_{ion} change upon the nanoparticle translocation by calculating the steady-state ion flux through a 300 nm SiN_x nanopore with a 180 nm nanosphere moving along the axial direction in a framework of a finite element method (**Figure 5**a).[43,46] Comparing the position-dependent ionic current with the measured resistive pulses (Figure 5b), we estimated the temporal changes in the particle location z (Figure 5c) as well as its first derivative (Figure 5d), i.e., the translocation speed v. It revealed a steady increase in v as the nanoparticle moved closer to the nanopore under low-V_b conditions, which can be interpreted as the accelerated electrophoretic motions via the focused electric field. While this naturally anticipates larger v under higher transmembrane voltages, the nanoparticle velocity at the entrance was shown to become lower with V_b (Figure 5e). After passing through the entrance, meanwhile, it starts to accelerate rapidly followed by deceleration at the exit via viscous dragging (Figure 5e,f). The overall features represent an unexpected role of glycerol to retard the electrophoretic motions of the nanobeads only at the nanopore entrance.

In this regard, it is noticeable that the fast-moving polystyrenes distort the glycerol-water solution confined between their surface and the nanopore wall at high shear rates amounting to over 10^3 s^{-1}, which is orders of magnitude larger than the conditions involved in macroscopic fluid systems.[47,48] Such an extreme condition would anticipate the emergence of non-Newtonian characteristics of the viscoelastic fluid such as shear thickening and thinning.[49,50] For example, the electrostatically drawn particle densified the hydrogen bond-mediated glycerol-water molecule networks[51,52] at the front space. This dilatancy raised the local viscosity during the capture stage to give a longer t_{on}. As the particle entered the pore, meanwhile, the high-density glycerol was dissociated by the excessively strong electrophoretic forces under the huge electric field over 2 MV m^{-1} (Figure S4, Supporting Information) thereby leading to the rapid rise in v via the associated reduction in the viscosity through a transition from dilatant to pseudoplastic characteristics of the fluid (Figure 5g).

To verify this, we performed nanoparticle detections in several different viscoelastic fluids. Polyethylene glycol (PEG) of molecular weight 200 was mixed with water at 20 vol%. The resistive pulse measurements were performed in the PEG solution containing 0.14 M NaCl, where we found increased asymmetry in the ionic signal profiles (**Figure 6**a) due to the retarded (accelerated) particle motions at the pore entrance (exit) under higher V_b (Figure 6b). The results were qualitatively the same in xanthan gum solution (0.1 wt. %) (Figure 6c,d). These findings suggest the rather universal mechanism of the asymmetric translocation motions of nanoparticles in viscous solution involving the high-shear rate-mediated dynamic change in the local viscosity in the nanopore.

3. Conclusion

Raising solution viscosity has proven useful for improving several important features of nanopore sensing without any tradeoffs. Applying higher transmembrane voltage, the electrophoretic motions at the pore entrance can be retarded via

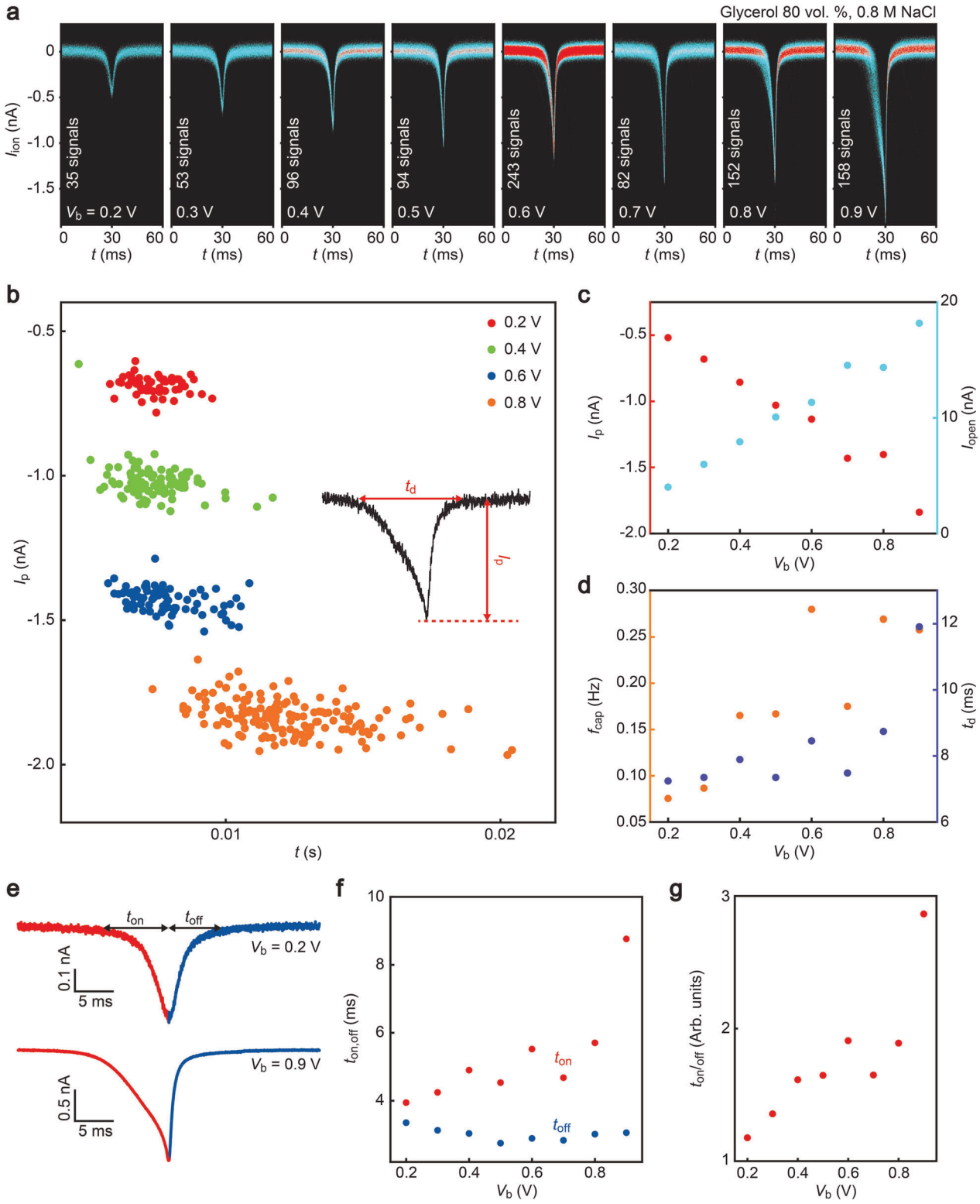

Figure 4. Transmembrane voltage contributions on the translocation dynamics asymmetry. a) Resistive pulses detected for 180 nm nanoparticles translocated through a 300 nm nanopore in 80 vol% glycerol solution of $\eta = 94$ mPa s containing 0.8 M NaCl under various V_b conditions. All the data were taken using one identical nanopore. b) Resistive pulse height (I_p) versus width (t_d) scatter plots. c) I_p (red) and I_{open} (skyblue) plotted against V_b. d) Transmembrane voltage dependence of the particle capture rate f_{cap} (orange) and translocation time (t_d). e) Typical resistive pulses obtained at 0.2 V (top) and 0.9 V (bottom). Red and blue colors denote the onsets and tails of the signals. f) Plots of t_{on} (red) and t_{off} (blue) as a function of V_b. g) V_b-dependence of the ratio between t_{on} and t_{off} exhibiting increased resistive pulse asymmetry under larger transmembrane voltage.

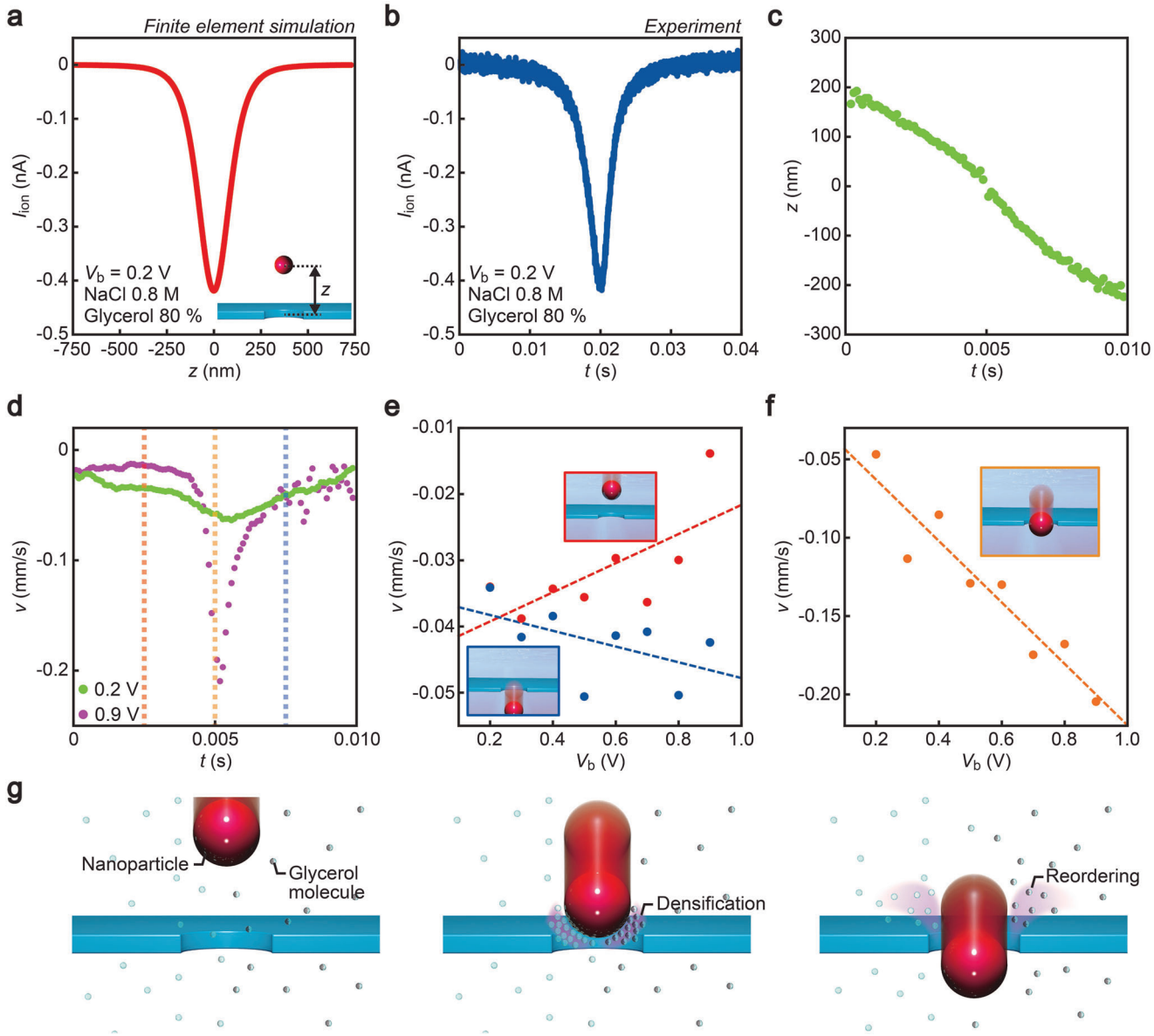

Figure 5. Velocimetric analysis of nanoparticle translocation dynamics in viscous solution. a) Ion blockade characteristics of a 180 nm nanosphere passing through a 300 nm nanopore in a 50 nm-thick SiN_x membrane in 0.8 M NaCl solution of viscosity 94 mPas under V_b = 0.2 V. z denotes the center position of the nanoparticle from the nanopore. b) A resistive pulse obtained under the same conditions in (a). c) Temporal change in the particle position deduced by comparing the $I_{ion} - z$ (a) and $I_{ion} - t$ (b) profiles. d) Nanoparticle velocity v numerically estimated from the $z - t$ traces under V_b = 0.2 V (green) and 0.9 V (purple). Orange dashed line points at the apex of the resistive pulses, while red and purple lines denote 2.5 ms before and after that point. e) The particle velocity 2.5 ms before (red) and after (blue) it passes through the nanopore. f) The translocation velocity at a point when the particle resides at the center of the nanopore. g) Conceptual models depicting the electrophoretic translocation mechanism of a nanoparticle in glycerol-water mixtures involving glycerol molecule densification and reordering under the influence of high shear rates within the nanoconfined liquid between the particle and the pore wall.

the dilatant characteristics of the shear-deformed nano-confined organic-water fluid. Simultaneously, it brings a more extensive electrostatic field to enable higher detection throughput by electrophoretically drawing a larger number of analytes into the sensing zone per unit time. Besides the capture-to-translocation dynamics, the increased voltage can also serve to amplify the ionic signals. All these outcomes of the combined use of viscous solution with high transmembrane voltage are beneficial for detecting small particles and molecules by the ionic current measurements, the task of which is generally difficult to accomplish by conventional means including a salt gradient approach that cannot serve to raise the signal-to-noise ratio.[25,53] Similar effects are expected in nanopores of different sizes by designing the experimental conditions to meet the shear rate requirement. Meanwhile, it should be noted that substances with small surface charge densities pass through a pore via electroosmotic flow

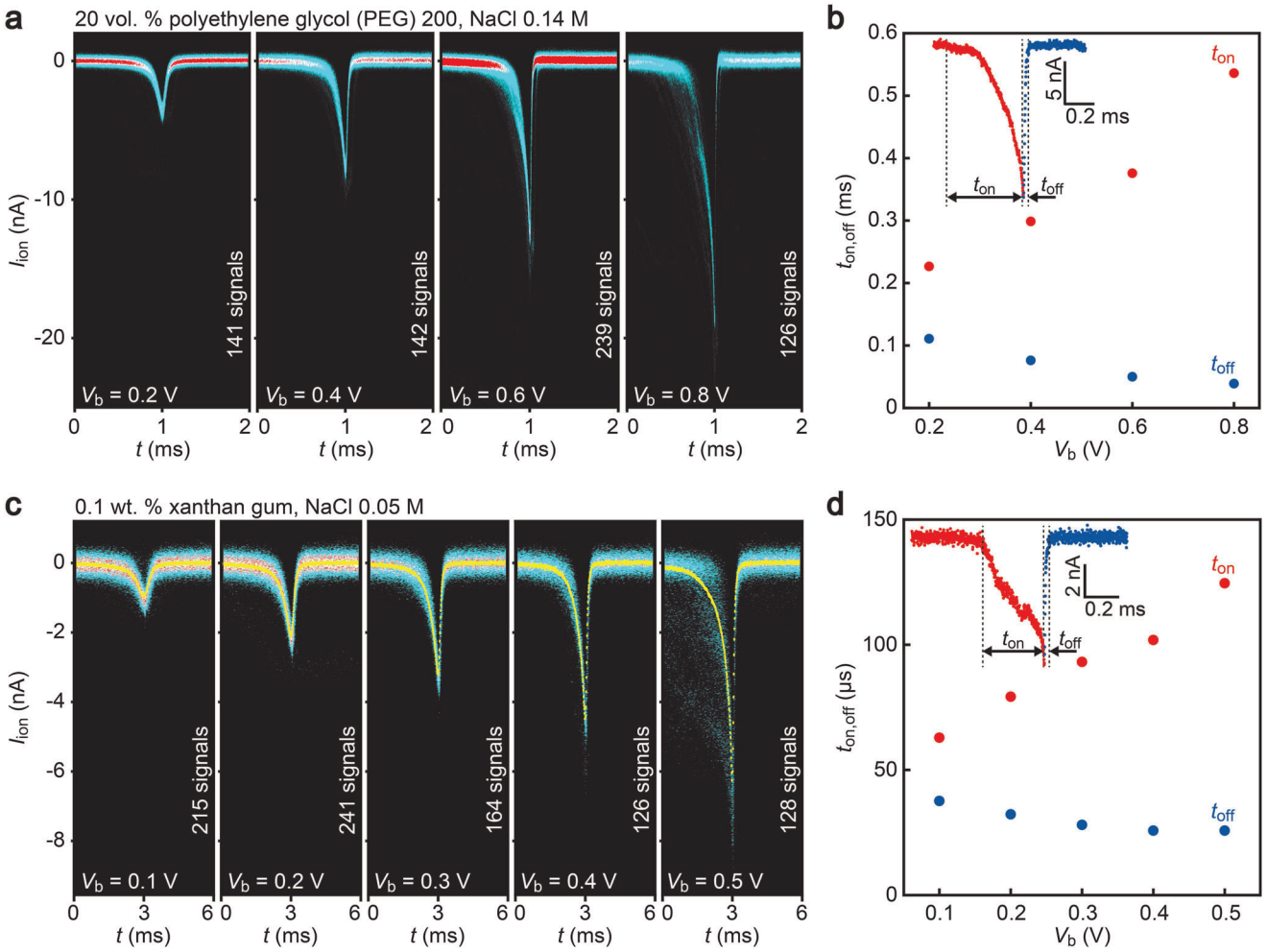

Figure 6. Asymmetric modes of translocation dynamics in other viscous solutions. a) Increase in resistive pulse asymmetry under higher transmembrane voltage for 180 nm nanoparticles translocating through a 300 nm nanopore in 20 vol% PEG (average molecular weight 200 g mol^{-1}) solution with 0.14 M NaCl. Yellow plots are the average I_{ion}. All the data were taken using one identical nanopore. b) Plots of t_{on} (red) and t_{off} (blue) as a function of V_b. c,d) Results for the nanoparticle translocation in 0.1 wt. % xanthan gum demonstrating similar features to those observed in the PEG and glycerol solutions. All the data were taken using one identical nanopore.

instead of electrophoresis.[54,55] Further efforts should be devoted to verifying whether the present approach equally works to slow down the translocation motions in such cases where the analytes are carried by the fluid flow.

4. Experimental Section

Polyimide-Covered Nanopore Chip Fabrications: A 4-inch silicon wafer was coated with 50 nm-thick silicon nitride layers on both sides by low-pressure chemical vapor deposition. A 1 mm × 1 mm region of the silicon nitride was removed through a metal mask by reactive ion etching using trifluoromethane etchant gas. The thus appeared silicon surface was exposed to 25% potassium hydroxide aq. heated to 80 °C. As a result, the silicon layer was anisotropically etched forming a deep trench with a 40 nm-thick silicon nitride membrane of approximately 200 μm × 200 μm size at the bottom. On the membrane surface, an electron beam resist ZEP520A was spin-coated and baked at 180 °C. Subsequently, a circle of diameter 300 nm was delineated by electron beam lithography. After development in a developer solution, the residual resist layer was used as a mask to open a nanopore by removing the exposed silicon nitride via the trifluoromethane reactive ion etching. After that, the nanopore chip was cleaned by keeping it in *N*,*N*-dimethylformamide overnight followed by rinsing with isopropanol and acetone several times. On the nanopore membrane, a 5 μm-thick photosensitive imide precursor was spin-coated and prebaked on a hot plate. The light was irradiated at a 50 μm region around the nanopore by mask-less photolithography followed by development and hard-baking. Finally, a silicon nitride nanopore was obtained in a 50 μm polyimide micropore. Here, the thick polymer layer served to reduce the chip capacitance thereby enabling a fast response of the ionic current against the particle translocation with suppressed high-frequency noise.

Flow Cell Integration: The entire surface of the polyimide except the area around the 50 μm-sized micropore was coated with 10 nm-thick silicon dioxide by chemical vapor deposition. On the silicon dioxide-coated polyimide surface, a microchannel-patterned polydimethylsiloxane (PDMS) block was bonded by pretreating their surfaces with oxygen plasma. The same process was used to adhere another piece of PDMS to the other side of the nanopore chip. Prior to the bonding, three holes were punched in each of the PDMS blocks, which were used for injecting

electrolyte solution into the nanopore as well as to insert Ag/AgCl rods for the ionic current measurements.

Ionic Current Characteristics Measurements: Glycerol was added to NaCl solution at various vol.% ratios for preparing electrolyte buffers of different viscosity at pH 7.4. The salt concentration was adjusted to make the ionic strength of the glycerol-water mixtures the same. The solution was poured into the holes in the PDMS blocks to fill the nanopore from both sides. An silver/silver chrolide electrode was used to apply the transmembrane voltage V_b and record the ionic current I_{ion} through the nanopore using a pico ammeter-source unit (Keithley 6487). I_{ion} versus V_b characteristics were measured by sweeping the voltage at a 5 mV step in a range from 1.4 to −1.4 V.

Single-Nanoparticle Detections: 180 nm-sized carboxylated polystyrene nanobeads (Polysciences) were dispersed in the salt solutions at 1×10^{10} particle mL^{-1}. The zeta potentials of the nanoparticles were measured to be around -40 mV using a zeta sizer (Malvern). The particle suspension was added to one side of the nanopore while filling the other side with the solution containing no nanoparticles. The transmembrane voltage V_b was applied to an Ag/AgCl electrode using a battery-based potentiostat. The output ionic current was recorded through another silver/silver chrolide electrode placed at the other side of the membrane by amplifying it with a custom-designed current amplifier followed by digitizing with a fast digitizer (NI PXI-5922) and data storage in a solid-state drive (NI HDD-8261) at 1 MHz. In order to avoid the influence of fabrication errors, the same nanopore chip was used to investigate the viscosity and voltage dependence of the nanoparticle translocation dynamics. For the variation in the nanopore structures, meanwhile, it was confirmed to cause only marginal effects on the measurement results (Figures S14 and S15, Supporting Information). All the measurements were performed under a program coded in LabVIEW.

Resistive Pulse Analyses: The I_{ion} traces were sectioned into 0.5 seconds of data. The base current in each data set was offset to zero by subtracting the linearly-fitted component. Resistive pulses in the offsetted I_{ion} curves were extracted by finding the local minima below a threshold level followed by saving 2500 points before and after the local minima in a data file. The onset (t_{on}) and offset time (t_{off}) were obtained by calculating the time required for the ionic current to reach above zero amperes from the pulse apexes. The resistive pulse heights were acquired as the minimal I_{ion} in each ionic signal. All the data analyses were performed using a program coded in Visual Basic.

Statistical Analysis: Distributions of the resistive pulse feature parameters such as the height, width, t_{on}, t_{off}, and Δt were evaluated by constructing histograms. Gaussian peaks were fit to the distributions to assess the average values and the variations as their center positions and the full width at half-maxima. All the calculations were performed using Origin Pro.

Finite Element Analyses: A three-dimensional model of a cylindrical pore of 300 nm diameter in a 50 nm-thick silicon nitride membrane (electrical conductivity of $\sigma = 1.4 \times 10^{-14}$ S m^{-1} and relative permittivity of $\varepsilon_r = 9.7$) was constructed in COMOSL Multiphysics 5.4. The whole geometrical structure consisted of an 8 µm-radius and 16.05 µm-height cylinder filled with a glycerol-water mixture of various viscosities from 1 mPas (0 vol%) to 94 mPas (80 vol%) with Na^+ and Cl^- at a concentration 1 mol L^{-1}. A sphere of diameter 180 nm was placed at a position along the axial direction. The transmembrane ionic current was calculated by solving the Poisson equation, continuity equation at steady-state current, Nernst-Planck equation, and Naiver-Stokes equation in a framework of a finite element method. All simulations were conducted by a software package of COMSOL multiphysics 5.4 using AC/DC, Chemical Reaction Engineering, and Computational Fluid Dynamics (CFD) modules.

Supporting Information

Supporting Information is available from the Wiley Online Library or from the author.

Acknowledgements

This work was supported by the Japan Society for the Promotion of Science (JSPS) KAKENHI Grant Number 22H01926 and 22K04893.

Conflict of Interest

The authors declare that they have no conflict of interest.

Data Availability Statement

The data that support the findings of this study are available in the supplementary material of this article.

Keywords

dilatancy, nanofluidics, nanopores, translocation dynamics

Received: November 3, 2023
Revised: April 26, 2024
Published online:

[1] T. Albrecht, *Ann. Rev. Anal. Chem.* **2019**, *12*, 371.
[2] L. Xue, H. Yamazaki, R. Ren, M. Wanunu, A. P. Ivanov, J. B. Edel, *Nat. Rev. Mater.* **2020**, *5*, 931.
[3] Y. Wu, J. J. Gooding, *Chem. Soc. Rev.* **2022**, *51*, 3862.
[4] Y. He, M. Tsutsui, Y. Zhou, X. S. Miao, *NPG Asia Mater* **2021**, *13*, 48.
[5] C. Wen, S. L. Zhang, *J. Appl. Phys.* **2021**, *129*, 064702.
[6] J. Houghtaling, C. Ying, O. M. Eggenberger, A. Fennouri, S. Nandivada, M. Acharjee, J. Li, A. R. Hall, M. Mayer, *ACS Nano* **2019**, *13*, 5231.
[7] J. P. Fried, J. L. Swett, B. P. Nadappuram, J. A. Mol, J. B. Edel, A. P. Ivanov, J. R. Yates, *Chem. Soc. Rev.* **2021**, *50*, 4974.
[8] R. Hu, X. Tong, Q. Zhao, *Adv. Health. Mater.* **2020**, *9*, 2000933.
[9] I. M. F. Tanimoto, B. Cressiot, S. J. Greive, B. L. Pioufle, L. Bacri, J. Pelta, *Nano Res.* **2022**, *15*, 9906.
[10] C. Plesa, S. W. Kowalczyk, R. Zinsmeester, A. Y. Grosberg, Y. Rabin, C. Dekker, *Nano Lett.* **2013**, *13*, 658.
[11] S. Kishimoto, S. Murayama, M. Tsutsui, M. Taniguchi, *ACS Sens.* **2020**, *5*, 1597.
[12] J. K. Rosenstein, M. Wanunu, C. A. Merchant, M. Drndic, K. L. Shepard, *Nat. Methods* **2012**, *9*, 487.
[13] C. Y. Lin, R. Fotis, Z. Xia, K. Kavetsky, Y. C. Chou, D. J. Niedzwiecki, M. Biondi, F. Thei, M. Drndic, *Nano Lett.* **2022**, *22*, 8719.
[14] S. Shekar, C.-C. Chien, A. Hartel, P. Ong, O. B. Clarke, A. Marks, M. Drndic, K. L. Shepard, *Nano Lett.* **2019**, *19*, 1090.
[15] R. Hu, R. Zhu, G. Wei, Z. Wang, Z.-Y. Gu, M. Wanunu, Q. Zhao, *Adv. Mater.* **2023**, *35*, 2211399.
[16] S. M. Iqbal, D. Akin, R. Bashir, *Nat. Nanotechnol.* **2007**, *2*, 243.
[17] A. Arima, I. H. Harlisa, T. Yoshida, M. Tsutsui, M. Tanaka, K. Yokota, T. W. Tonomura, J. Yasuda, M. Taniguchi, T. Washio, M. Okochi, T. Kawai, *J. Am. Chem. Soc.* **2018**, *140*, 16834.
[18] S. van Dorp, U. F. Keyser, N. H. Dekker, C. Dekker, S. G. Lemay, *Nat. Phys.* **2009**, *5*, 347.
[19] M. Chinappi, M. Yamaji, R. Kawano, F. Cecconi, *ACS Nano* **2020**, *14*, 15816.
[20] M. Firnkes, D. Padone, J. Knezevic, M. Doblinger, U. Rant, *Nano Lett.* **2010**, *10*, 2162.
[21] D. Fologea, J. Uplinger, B. Thomas, D. S. McNabb, J. Li, *Nano Lett.* **2005**, *5*, 1734.

[22] S. R. German, T. S. Hurd, H. S. White, T. L. Mega, *ACS Nano* **2015**, *9*, 7186.
[23] O. M. Eggenberger, C. Ying, M. Mayer, *Nanoscale* **2019**, *11*, 19636.
[24] J. Saharia, Y. M. N. D. Y. Bandara, B. I. Karawdeniya, C. Hammond, G. Alexandrakis, M. J. Kim, *RSC Adv.* **2021**, *11*, 24398.
[25] M. Wanunu, W. Morrison, Y. Rabin, A. Y. Grosberg, A. Meller, *Nat. Nanotechnol.* **2010**, *5*, 160.
[26] N. D. Fiori, A. Squires, D. Bar, T. Gilboa, T. D. Moustakas, A. Meller, *Nat. Nanotechnol.* **2013**, *8*, 946.
[27] M. Tsutsui, S. Ryuzaki, K. Yokota, Y. He, T. Wahio, K. Tamada, T. Kawai, *Commun. Mater.* **2021**, *2*, 29.
[28] M. Zhang, C. Ngampeerapong, D. Redin, A. Ahmadian, I. Sychugov, J. Linnros, *ACS Nano* **2018**, *12*, 4574.
[29] C. Chau, F. Marcuccio, D. Soulias, M. A. Edwards, A. Tuplin, S. E. Radford, E. Hewitt, P. Actis, *ACS Nano* **2022**,*16*, 20075.
[30] S. Acharya, A. Jian, C. Kuo, R. Nazarian, K. Li, A. Ma, B. Siegal, C. Toh, J. J. Schmidt, *ACS Nano* **2020**, *2*, 370.
[31] S. Confederat, S. Lee, S. Vang, D. Soulias, F. Marcuccio, T. Il. Peace, M. A. Edwards, P. Strobbia, D. Samanta, C. Walti, P. Actis, *Small* **2024**, *20*, 2305186.
[32] Y. Qiu, Z. S. Siwy, M. Wanunu, *Anal. Chem.* **2019**, *91*, 996.
[33] C. C. Chau, S. E. Radford, E. W. Hewitt, P. Actis, *Nano Lett.* **2020**, *20*, 5553.
[34] S. Khatri, P. Pandey, G. Mejia, G. Ghimire, F. Leng, J. He, *J. Am. Chem. Soc.* **2023**, *145*, 28075.
[35] M. Tsutsui, K. Yokota, W. L. Hsu, D. Garoli, H. Daiguji, T. Kawai, *Device* **2024**, *2*, 100188.
[36] N.-S. Cheng, *Ind. Eng. Chem. Res.* **2008**, *47*, 3285.
[37] S. Garaj, W. Hubbard, A. Reina, J. Kong, D. Branton, J. A. Gorovchenko, *Nature* **2010**, *467*, 190.
[38] C. Lee, L. Joly, A. Siria, A.-L. Biance, R. Fulcrand, L. Bocquet, *Nano Lett.* **2012**, *12*, 4037.
[39] W.-J. Lan, D. A. Holden, B. Zhang, H. S. White, *Anal. Chem.* **2011**, *83*, 3840.
[40] K. Bacri, A. G. Oukhaled, B. Schiedt, G. Patriarche, E. Bouehis, J. Gierak, J. Pelta, L. Auvray, *J. Phys. Chem. B* **2011**, *115*, 2890.
[41] S. W. Kowalczyk, A. Y. Grosberg, Y. Rabin, C. Dekker, *Nanotechnology* **2011**, *22*, 315101.
[42] V. Tabard-Cossa, D. Trivedi, M. Wiggin, N. N. Jetha, A. Marziali, *Nanotechnology* **2007**, *18*, 305505.
[43] M. Tsutsui, K. Yokota, A. Arima, Y. He, T. Kawai, *ACS Sens.* **2019**, *4*, 2974.
[44] M. Charron, K. Briggs, S. King, M. Waugh, V. Tabard-Cossa, *Anal. Chem.* **2019**, *91*, 12228.
[45] F. Marcuccio, D. Soulias, C. C. C. Chau, S. E. S. E. Radford, E. Hewitt, P. Actis, M. A. Edwards, *ACS Nanosci. Au* **2023**, *3*, 172.
[46] C. Liao, F. Antaw, A. Wuethrich, W. Anderson, M. Trau, *Small Struct* **2020**, *1*, 2000011.
[47] K. Schroter, E. Donth, *J. Chem. Phys.* **2000**, *113*, 9101.
[48] S. W. Sofie, F. Dogan, *J. Am. Ceram. Soc.* **2001**, *84*, 1459.
[49] M. Wei, K. Lin, L. Sun, *Mater. Design* **2022**, *216*, 110570.
[50] B. Kim, S. Kwon, M. Lee, Q. Kim, S. An, W. Jhe, *Proc. Natl. Acad. Sci* **2015**, *112*, 15619.
[51] T. R. Fisher, G. Zhou, Y. Shi, L. Huang, *Phys. Chem. Chem. Phys.* **2020**, *22*, 2887.
[52] K. Dziubinska-Kuhn, M. Pupier, J. Matysik, J. Viger-Gravel, B. Karg, M. Kowalska, *Chem. Phys. Chem.* **2022**, *23*, 202100806.
[53] M. Charron, L. Philipp, L. He, V. Tabard-Cossa, *Nano Res.* **2022**, *15*, 9943.
[54] B. I. Karawdeniya, Y. M. N. D. Y. Bandara, A. I. Khan, W. T. Chen, H.-A. Vu, A. Morshed, J. Suh, P. Dutta, M. J. Kim, *Nanoscale* **2020**, *12*, 23721.
[55] Y. M. Nuwan, D. Y. Bandara, K. J. Freedman, *ACS Nano* **2022**, *16*, 14111.

